 doi:10.20944/preprints202209.0270.v1

Communication

A Comparative Investigation on Mechanical Properties of Tib_2/Cr Multilayer Film by Indentation

Simeng Chen [1], Zhengtao Wu [1,*], Qimin Wang [1,2,*]

[1] School of Electromechanical Engineering, Guangdong University of Technology, 510006 Guangzhou, China
[2] Key Laboratory of Green Fabrication and Surface Technology of Advanced Metal Materials (Anhui University of Technology), Ministry of Education, Maanshan 243002, China
* Correspondence: ztwu@gdut.edu.cn, qmwang@gdut.edu.cn

Abstract: Alternating TiB_2-dcMS and Cr-HiPIMS layers are used to fabricate TiB_2/Cr multilayer films. Introducing a 5-nm-thick Cr interlayer deposited under a substrate bias of -60 V produces slight increases of both film hardness and elastic modulus. The TEM observation indicates that the Cr grains favor epitaxially growth on TiB_2 interlayer, forming a coherent TiB_2/Cr interface. This produces the hardness increasement. Mechanic measurement by using AFM illustrates that the coherent interface increases the elastic modulus of the Cr up to ~280 GPa, which is significantly higher than bulk material.

Keywords: TiB_2/Cr; Multilayer; Mechanical properties; Coherent interface

1. Introduction

Plenty of reported works on multilayer films focused on nitride-based materials attract great interest as superhard films and wear-resistance applications. Film properties including hardness, toughness, adhesive strength, and wear resistance are enhanced by incorporating nanocrystalline multilayer structure [1-5]. These multilayered structures consist of repeating interlayers of two different materials with nanometer-scale thicknesses. Compared to monolayer films, nanomultilayer films have superior mechanical properties. For example, Sun et al. [6] prepared TiAlN/TiB_2 multilayer films and found that all multilayer films with well-defined interfaces showed higher hardness than the individual TiAlN and TiB_2 layers. It was reported that the increase of hardness is not only due to the laminar structure and its different shear moduli, but also due to the mismatch of lattice constants at adjacent interfaces, which creates tensile stress fields and compressive stress fields, and the forces generated by the two materials with different shear moduli impede the dislocation motion when the dislocation crosses the coherent interface [7]. In general, theories including interface coordinated strain theory, coherent epitaxy theory, Hall-patch reinforcement effect, and interface composite theory have been used to demonstrate the mechanism behind the hardness improvement [8-11].

TiB_2 has been wildly used for wear parts, seals, cutting tools, and metal matrix composites due to its high hardness and wear resistance [12]. Multilayering TiB_2 with metallics (such as Cr [13], Ti [14], FeMn [15]), carbides and nitrides (such as TiAlN [16], TiN [17], TiC [18, 19], VC [20], BN [21]), oxides (such as Al_2O_3 [22]), and carbon-based layers [23] have been reported to further improve the mechanical properties of the TiB_2. In our recent work [24], alternating TiB_2-dcMS and Cr-HiPIMS layers are used to fabricate TiB_2/Cr multilayer films with varying the Cr interlayer thickness, 2 and 5 nm, and the substrate bias during growth of Cr interlayers from floating, to -60 V and -200 V. The results reveal that increasing the substrate bias during Cr interlayer growth from floating to -60 V produces increases of both film hardness and elastic modulus. However, the atomic-scale microstructure of the TiB_2/Cr interface is still unknown. The impact of the interface on film

Preprints (www.preprints.org) | NOT PEER-REVIEWED | Posted: 19 September 2022 doi:10.20944/preprints202209.0270.v1

hardness enhancement and the evolution of the mechanical properties of the Cr interlayer are not clear as well.

Therefore, an analytical TEM study was performed to obtain a structural insight into the TiB_2/Cr interface in this work. Mechanical-property measurements of the TiB_2/Cr multilayer film by nanoindentation using constant load mode and continuous-stiffness method (CSM) were applied. In addition, the film cross-section was mechanically characterized using AFM (atomic force microscopy). A comparative investigation on mechanical properties of the TiB_2/Cr multilayer film by indentation was conducted.

2. Materials and methods

A hybrid configuration of HiPIMS (high-power-impulse-magnetron sputtering) and dcMS (direct current magnetron sputtering) was employed to fabricate the TiB_2/Cr multilayer film. Schematic diagram of the configuration was illustrated in Fig. 1(a). The Cr target is operated in HiPIMS mode and dc power is applied to the TiB_2 targets (Cr-HiPIMS/TiB_2-dcMS). Prior to deposition, the 15 × 15 mm^2 Si(001) and WC-Co (6 wt% Co) substrates were cleaned in acetone and isoacetone successively. During deposition, the total system pressure was 3 mTorr (0.4 Pa) and the substrates were heated using a resistance heater with a temperature of 500 °C during deposition measured by a thermocouple mounted next to the substrate. To ensure better adhesion of the TiB_2 coating, a 30 nm Cr buffer layer was first deposited on the substrate by HiPIMS. The Cr-HiPIMS power was constant at 1.5 kW (200 Hz, 50 μs pulse length, duty cycle of 1%), deposition time 30 s. however, the TiB_2-dcMS- power was stable at 2.0 kW, deposition time 5 min, alternate in turn for twenty cycles. A detailed description of the film deposition was reported in previous work. A 5-nm-thick Cr interlayer deposited under a substrate bias of -60 V was selected to fabricate the multilayer. Schematic diagram of the multilayer structure was illustrated in Fig. 1(b). Fig. 1(c) presents the θ-2θ XRD pattern of the TiB_2/Cr multilayer film. The film has hexagonal crystal structure characteristic of TiB_2 (JCPDS No. 35-0741).

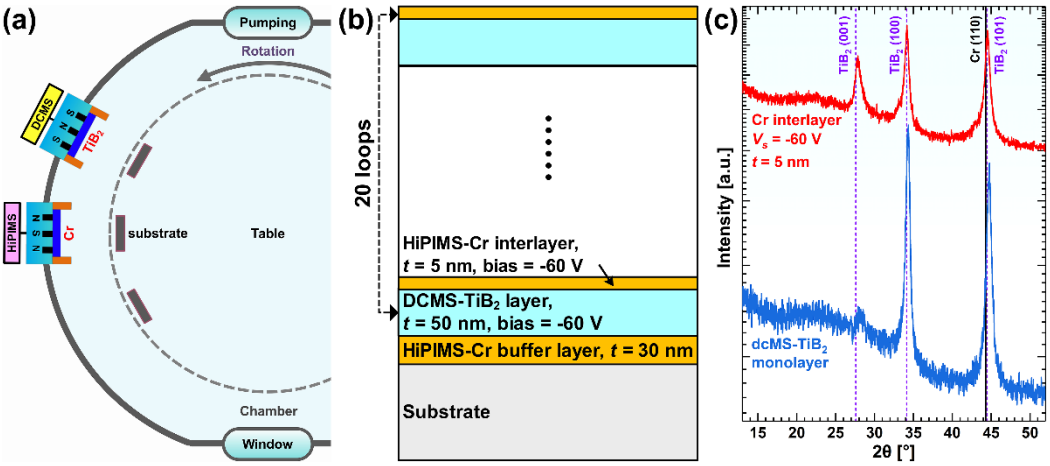

Fig. 1. Schematic diagrams of (a) Cr-HiPIMS/TiB_2-dcMS sputtering deposition system and (b) TiB_2/Cr multilayer. (c) presents θ-2θ XRD patterns of TiB_2/Cr multilayer film.

The film crystal structure was detected using a Philips Panalytical X'Pert PRO X-ray diffraction system (XRD, D8 Advance Diffractometer, Bruker) operated with Cu K_α (λ = 0.154 nm) radiation. The scanning range is 20° to 80° with a scanning step of 0.02° and a dwell time of 0.1 s/step. Film morphologies were investigated using cross-sectional scanning electron microscopy (XSEM Nano 430, FEI) operated at 10 kV and cross-sectional transmission electron microscope (XTEM Tecnai G^2 F20) with 200 kV accelerated voltage analyses. A Berkovich diamond tip (Ø 20 μm) in an Anton-Paar-TriTec UNHT^3 instrument was used to determine the mechanical properties of the film. Both the constant load mode under a constant loading of 10 mN and the continuous-stiffness method with the max load 20 mN and amplitude 10% were used to determine the hardness (H) and elastic modulus

Preprints (www.preprints.org) | NOT PEER-REVIEWED | Posted: 19 September 2022 doi:10.20944/preprints202209.0270.v1

(E) of the multilayer film as a function of the maximum load and penetration depth. In addition, the elastic modulus of the film cross-section was characterized using AFM in a Park NX20 machine. It works on the following principles: A micro-cantilever, which is extremely sensitive to weak forces, is fixed at one end and has a tiny needle tip (Diamond material) at the other end which is in gentle contact with the sample surface. This force causes the cantilever to deflect due to the very weak repulsive forces between the atoms at the tip of the needle and the atoms on the sample surface. The laser beam generated by the laser diode is focused through the lens onto the back of the cantilever and then reflected back to the photodiode to form the feedback. As the sample is scanned, the sample moves slowly on the carrier table and the micro-cantilever is adjusted by the feedback adjustment system to bend and undulate in response to the surface profile of the sample, the reflected beam is then deflected and the surface profile and mechanical information is recorded by the detector.

3. Results and discussion

Figure 2 shows XSEM and XTEM images of the surface and cross-section of the TiB_2/Cr multilayer film. The film surface is smooth. Both XSEM and XTEM images indicate that the 1.1-μm-thick multilayer film is dense without cracks or pores in the film cross-section. The TiB_2/Cr interface appears sharp and the TiB_2 interlayers have a columnar structure. In Fig. 2(e), it was deduced that low angle (5°) grain boundaries were formed between the TiB_2 and the Cr nanograins. The Cr grains favor epitaxially growth on TiB_2 interlayer, forming a coherent TiB_2/Cr interface.

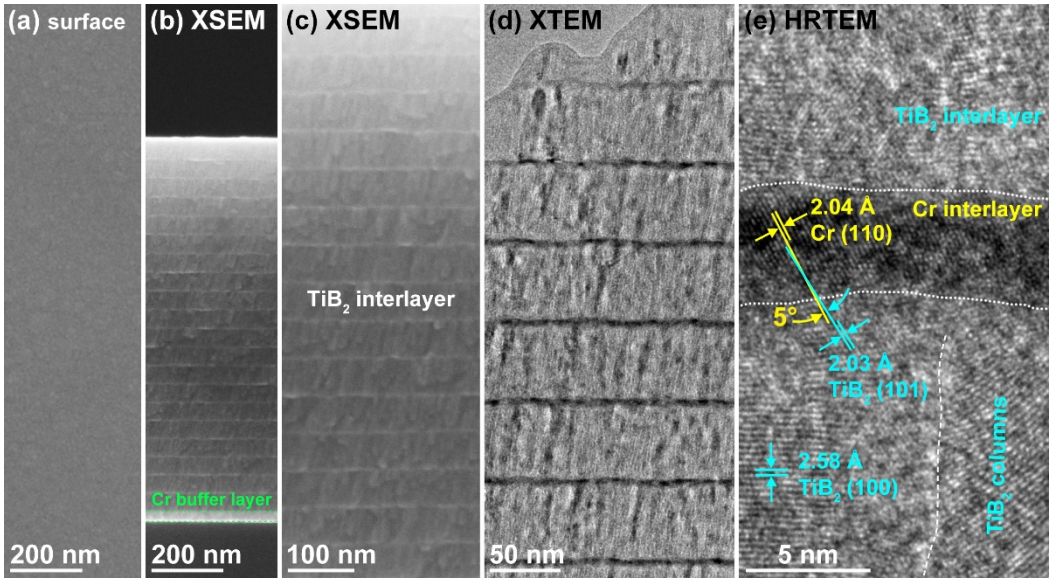

Fig. 2. (a) SEM surface, (b, c) SEM cross-section, (d) XTEM, and (e) HRTEM images of the TiB_2/Cr multilayer film.

Figure 3(a) exhibits load-penetration depth curves of nanoindentation tests (constant load mode, max. load 10 mN) applied on film surface. The max. penetration depth of the indenter was ~110 nm (~10% of film thickness). The film hardness and elastic modulus were 28.8 ± 0.8 and 395 ± 12 GPa, respectively. A dcMS-TiB_2 monolayer has a hardness of 27.9 ± 0.8 GPa and an elastic modulus of 340 ± 6 GPa [24]. Introducing a 5-nm-thick Cr interlayer deposited under a substrate bias of -60 V produces increases of both film hardness and elastic modulus. Fig. 3(b) presents load vs. time curve of penetrated indenter using continuous stiffness measurement mode. The max. load was 20 mN and amplitude was ~10% of the real-time load. Fig. 3(c) shows H and E values determined by CSM-mode measurement as a function of the penetration depth. A continuous increase of hardness and decrease of elastic modulus occurred as the penetration depth increases. This could

Preprints (www.preprints.org) | NOT PEER-REVIEWED | Posted: 19 September 2022 doi:10.20944/preprints202209.0270.v1

be due to an indentation size effect whereby the measured hardness increases with increasing indentation load [25]. The effect has been attributed to a variety of contributions including the elastic recovery of the indentation, surface dislocation pinning, dislocation nucleation, deformation band spacing, surface energy of the test specimen, and statistical measurement errors. Residual stress may also influence measured hardness values.

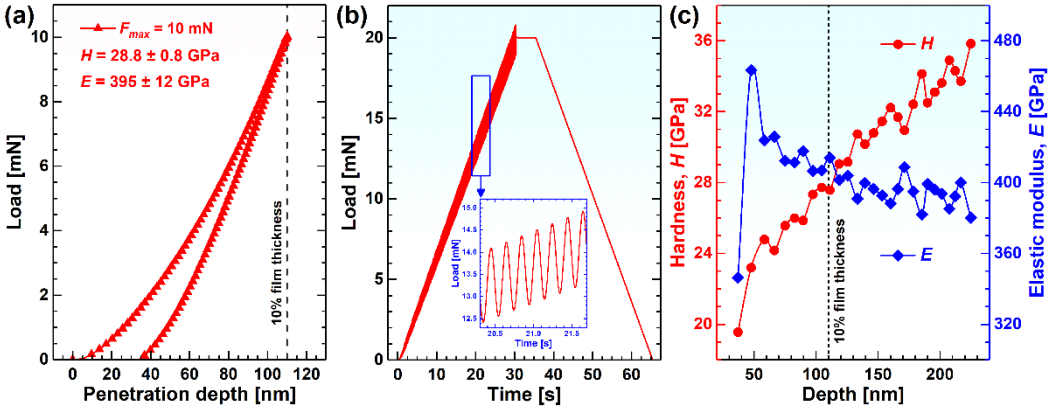

Fig. 3. (a) exhibits load-penetration depth curves of nanoindentation tests applied on film surface (constant load mode, max. load 10 mN), (b) presents load vs. time curve of penetrated indenter using continuous stiffness measurement mode, and (c) shows CSM-mode determined H and E values as a function of the penetration depth.

We try to calculate the average grain sizes of these films using TiB_2 (100) XRD peaks. The results are listed in Table 1. We can find that the Cr layer introduction has slight impact on average grain sizes of TiB_2. In addition, a slight shift to the lower 2θ values is present in multilayer film with respect to the monolayer film which indicates a change in the stress state (Fig. 2b). Based on the fact that the multilayer films' peak match the bulk value, one may assume that the reference TiB_2 film is in slight state of tension. The hardness of the reference TiB_2 monolayer film is slightly improved by Cr interlayer introduction. Hardness increases from 27.9 ± 0.8 GPa for TiB_2 monolayer to 28.8 ± 0.8 GPa for the TiB_2/Cr film with 5 nm Cr interlayer deposited at -60 V bias (Fig. 3a). Therefore, we can make conclusion that the change in the stress state (from tension to compressive) induces a slight increase of film hardness.

Table S1 Average grain sizes of dcMS-TiB_2 monolayer and TiB_2/Cr multilayer films.

Samples	Cr layer thickness [nm]	Cr substrate bias [V]	Average grain sizes of TiB_2 [nm]
TiB_2 monolayer	0	-	15.7
TiB_2/Cr multilayer	5	-60	15.1

In addition, it was noticed that the Cr grains favor epitaxially growth on TiB_2 interlayer, forming a coherent TiB_2/Cr interface. This produces the hardness increasement compared to a monolayer as well. Mechanical characterization by using AFM was conducted to investigate the evolution of the mechanical properties of the Cr interlayer, as shown in Fig .4. Fig.4(a) shows 50-nm thickness of TiB_2 interlayer and 5-nm thickness of Cr interlayer. Fig.4(b) shows AFM morphology of the polished film cross-section. An alternating TiB_2/Cr multilayer structure was notice since the relatively soft Cr layer was much easier to be removed compared to hard TiB_2 layer. The measurement by AFM shows that the elastic modulus of the Cr was ~280 GPa, which is significantly higher than magnetron-sputtered Cr monolayer (~165 GPa [26, 27]). Thus, the coherent TiB_2/Cr interface increases mechanical properties of both the TiB_2 and the Cr interlayers.

 doi:10.20944/preprints202209.0270.v1

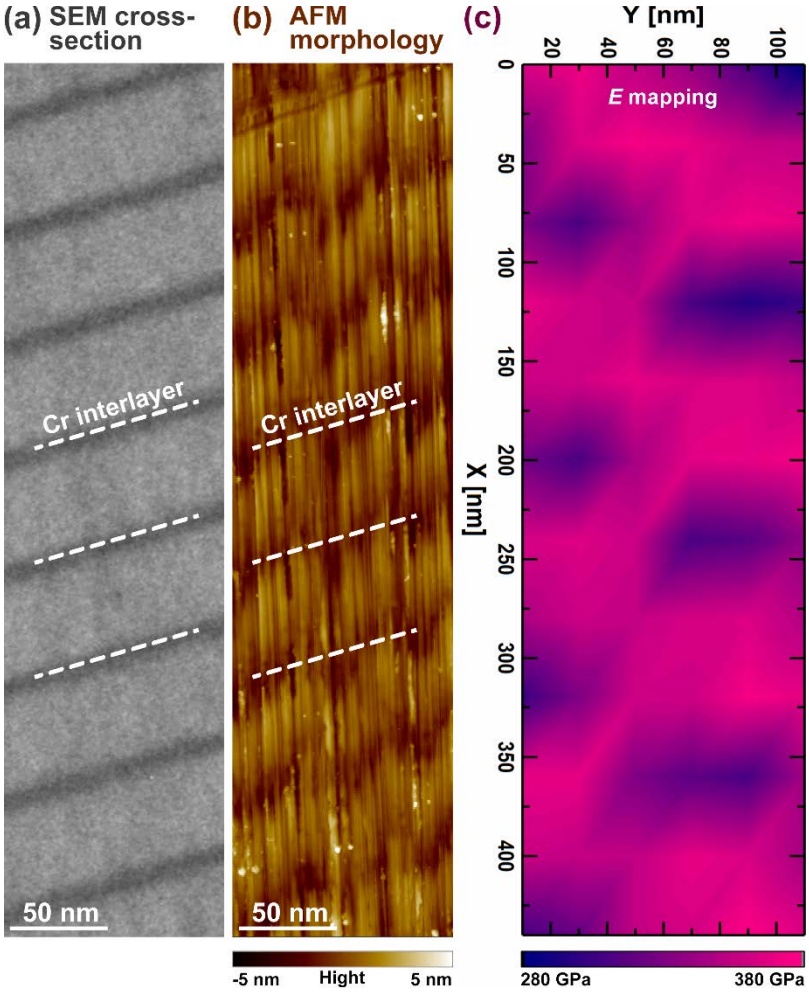

Fig. 4. Elastic modulus characterization of the TiB_2/Cr multilayer film using AFM. (a) exhibits cross-section morphology of the film. (b) shows height of the film cross-section. (c) presents elastic modulus E mapping of the film cross-section.

4. Conclusions

TiB_2/Cr multilayer film was fabricated using Cr-HiPIMS/TiB_2-dcMS hybrid deposition. The Cr layer introduction has slight impact on average grain sizes of TiB_2. The Cr grains favor epitaxially growth on TiB_2 interlayer, forming a coherent TiB_2/Cr interface. This produces the change in the stress state (from tension for monolayer to compressive for multilayer) induces a slight increase of film hardness. The hardness and the elastic modulus of the TiB_2/Cr multilayer film were 28.8 ± 0.8 and 395 ± 12 GPa, respectively. Introducing a 5-nm-thick Cr interlayer deposited under a substrate bias of -60 V produces increases of both film hardness and elastic modulus compared to those of a dcMS-TiB_2 monolayer because of the coherent interface and compressive-stress state. The coherent interface results in the strengthening of Cr interlayer as well, which has a high elastic modulus of ~280 GPa.

Acknowledgements

The authors gratefully acknowledge the financial support of the National Key Research and Development Project of China (2017YFE0125400) and the National Natural Science Foundation of China (51901048). This work was partly supported by the open project of Key Laboratory of Green Fabrication and Surface Technology of Advanced Metal Materials (GFST2020KF06).

References

1. Skordaris, G.; Bouzakis, K.-D.; Kotsanis, T.; Charalampous, P.; Bouzakis, E.; Lemmer, O.; Bolz, S., Film thickness effect on mechanical properties and milling performance of nano-structured multilayer PVD coated tools. *Surf. Coat. Technol.* **2016,** *307*, 452-460.
2. Yang, W.; Ayoub, G.; Salehinia, I.; Mansoor, B.; Zbib, H., Deformation mechanisms in Ti/TiN multilayer under compressive loading. *Acta Mater.* **2017,** *122*, 99-108.
3. Ghailane, A.; Makha, M.; Larhlimi, H.; Alami, J., Design of hard coatings deposited by HiPIMS and dcMS. *Mater. Lett.* **2020,** *280*, 128540.
4. Bagdasaryan, A. A.; Pshyk, A. V.; Coy, L. E.; Kempiński, M.; Pogrebnjak, A. D.; Beresnev, V. M.; Jurga, S., Structural and mechanical characterization of (TiZrNbHfTa)N/WN multilayered nitride coatings. *Mater. Lett.* **2018,** *229*, 364-367.
5. Santaella-González, J. B.; Hernández-Torres, J.; Morales-Hernández, J.; Flores-Ramírez, N.; Ferreira-Palma, C.; Rodríguez-Jiménez, R. C.; García-González, L., Effect of the number of bilayers in Ti/TiN coatings on AISI 316L deposited by sputtering on their hardness, adhesion, and wear. *Mater. Lett.* **2022,** *316*, 132037.
6. Sun, Y.; Yan, J.; Zhang, S.; Xue, F.; Liu, G.; Li, D., Influence of modulation periods and modulation ratios on the structure and mechanical properties of nanoscale TiAlN/TiB_2 multilayers prepared by IBAD. *Vacuum* **2012,** *86* (7), 949-952.
7. Li, B.; Ma, X.; Li, W.; Zhai, Q.; Liu, P.; Zhang, K.; Ma, F., Effect of SiC thickness on microstructure and mechanical properties of (AlCrTiZrV) N/SiC nano-multilayers film synthesized by reactive magnetron sputtering. *Thin Solid Films* **2021,** *730*, 138724.
8. Zuo, B.; Xu, J.; Lu, G.; Ju, H.; Yu, L., Microstructures, mechanical properties and corrosion resistance of TiN/AlN multilayer films. *Ceram. Int.* **2022,** *48* (*8*), 11629-11635.
9. Yang, M.; Liu, Y.; Fan, T.; Zhang, D., Metal-graphene interfaces in epitaxial and bulk systems: A review. *Prog. Mater. Sci.* **2020,** *110*, 100652.
10. Carpenter, J. S.; Misra, A.; Anderson, P. M., Achieving maximum hardness in semi-coherent multilayer thin films with unequal layer thickness. *Acta Mater.* **2012,** *60* (6-7), 2625-2636.
11. Zhang, Y.; Xue, S.; Li, Q.; Li, J.; Ding, J.; Niu, T.; Su, R.; Wang, H.; Zhang, X., Size dependent strengthening in high strength nanotwinned Al/Ti multilayers. *Acta Mater.* **2019,** *175*, 466-476.
12. Gurusamy, P.; Prabu, S. B.; Paskaramoorthy, R., Influence of processing temperatures on mechanical properties and microstructure of squeeze cast aluminum alloy composites. *Mater. Manuf. Processes* **2015,** *30* (3), 367-373.
13. Dai, W.; Li, X.; Wang, Q., Microstructure and properties of TiB_2/Cr multilayered coatings with double periodical structures. *Surf. Coat. Technol.* **2020,** *382*, 125150.
14. Sheng, L.; Xiao, Y.; Jiao, C.; Du, B.; Li, Y.; Wu, Z.; Shao, L., Influence of layer number on microstructure, mechanical properties and wear behavior of the TiN/Ti multilayer coatings fabricated by high-power magnetron sputtering deposition. *J. Manuf. Processes* **2021,** *70*, 529-542.
15. Wang, C.; Han, J.; Pureza, J. M.; Chung, Y.-W., Structure and mechanical properties of $Fe_{1-x}Mn_x$/TiB_2 multilayer coatings: Possible role of transformation toughening. *Surf. Coat. Technol.* **2013,** *237*, 158-163.
16. Sun, Y.; Li, D.; Gao, C.; Wang, N.; Yan, J.; Dong, L.; Cao, M.; Deng, X.; Gu, H.; Wan, R., The effect of annealing on hardness, residual stress, and fracture resistance determined by modulation ratios of TiB_2/TiAlN multilayers. *Surf. Coat. Technol.* **2013,** *228*, S385-S388.
17. Naeem, M.; Awan, S.; Shafiq, M.; Raza, H.; Iqbal, J.; Díaz-Guillén, J.; Sousa, R.; Jeelani, M.; Abrar, M., Wear and corrosion studies of duplex surface-treated AISI-304 steel by a combination of cathodic cage plasma nitriding and PVD-TiN coating. *Ceram. Int.* **2022**.
18. Chitsaz-Khoyi, L.; Khalil-Allafi, J.; Motallebzadeh, A.; Etminanfar, M., The effect of hydroxyapatite nanoparticles on electrochemical and mechanical performance of TiC/N coating fabricated by plasma electrolytic saturation method. *Surf. Coat. Technol.* **2020,** *394*, 125817.
19. Kim, H. S.; Kang, B. R.; Choi, S. M., Fabrication and characteristics of a HfC/TiC multilayer coating by a vacuum plasma spray process to protect C/C composites against oxidation. *Corros. Sci.* **2021,** *178*, 109068.
20. Wang, C.; Pureza, J. M.; Yang, Y.; Chung, Y.-W., Investigation of hardness and fracture toughness properties of Fe/VC multilayer coatings with coherent interfaces. *Surf. Coat. Technol.* **2016,** *288*, 179-184.
21. Dong, L.; Li, D.; Zhang, S.; Yan, J.; Liu, M.; Gao, C.; Wang, N.; Liu, G.; Gu, H.; Wan, R., Microstructure and mechanical properties of as-deposited and annealed TiB_2/BN superlattice coatings. *Thin Solid Films* **2012,** *520* (16), 5328-5332.

22. He, X.; Dong, L.; Wu, J.; Li, D., The influence of varied modulation ratios on crystallization and mechanical properties of nanoscale TiB_2/Al_2O_3 multilayers. *Surf. Coat. Technol.* **2019,** *365*, 65-69.
23. Rao, J.; Cruz, R.; Lawson, K.; Nicholls, J., Sputtered DLC-TiB_2 multilayer films for tribological applications. *Diamond Relat. Mater.* **2005,** *14* (11-12), 1805-1809.
24. Wu, Z.; Ye, R.; Bakhit, B.; Petrov, I.; Hultman, L.; Greczynski, G., Improving oxidation and wear resistance of TiB_2 films by nano-multilayering with Cr. *Surf. Coat. Technol.* **2022,** *436*, 128337.
25. Mattucci, M.; Cherubin, I.; Changizian, P.; Skippon, T.; Daymond, M., Indentation size effect, geometrically necessary dislocations and pile-up effects in hardness testing of irradiated nickel. *Acta Mater.* **2021,** *207*, 116702.
26. Ferreira, F.; Serra, R.; Oliveira, J. C.; Cavaleiro, A., Effect of peak target power on the properties of Cr thin films sputtered by HiPIMS in deep oscillation magnetron sputtering (DOMS) mode. *Surf. Coat. Technol.* **2014,** *258*, 249-256.
27. Cho, K.-H.; Kim, Y., Elastic modulus measurement of multilayer metallic thin films. *J. Mater. Res.* **1999,** *14* (5), 1996-2001.